

Exploring the Structure of the Bound Proton with Deeply Virtual Compton Scattering

M. Hattawy,^{1,22,32} N.A. Baltzell,^{1,32,38} R. Dupré,^{1,22} S. Bültmann,³² R. De Vita,¹⁹ A. El Alaoui,^{1,39} L. El Fassi,^{1,28} H. Egiyan,³⁸ F.X. Girod,³⁸ M. Guidal,²² K. Hafidi,¹ D. Jenkins,⁴² S. Liuti,⁴³ Y. Perrin,²⁷ S. Stepanyan,³⁸ B. Torayev,³² E. Voutier,^{22,27} S. Adhikari,¹² Giovanni Angelini,¹⁵ C. Ayerbe Gayoso,⁴⁴ L. Barion,¹⁷ M. Battaglieri,¹⁹ I. Bedlinskiy,²³ A.S. Biselli,¹⁰ F. Bossù,⁶ W. Brooks,³⁹ F. Cao,⁸ D.S. Carman,³⁸ A. Celentano,¹⁹ P. Chatagnon,²² T. Chetry,³¹ G. Ciullo,^{17,11} L. Clark,⁴⁰ P.L. Cole,^{26,16} M. Contalbrigo,¹⁷ V. Crede,¹³ A. D'Angelo,^{20,34} N. Dashyan,⁴⁵ E. De Sanctis,¹⁸ M. Defurne,⁶ A. Deur,³⁸ S. Diehl,⁸ C. Djalali,^{31,36} M. Ehrhart,²² P. Eugenio,¹³ S. Fegan,^{40,*} A. Filippi,²¹ T.A. Forest,¹⁶ A. Fradi,^{22,†} M. Garçon,⁶ G. Gavalian,^{38,32} N. Gevorgyan,⁴⁵ G.P. Gilfoyle,³³ K.L. Giovanetti,²⁴ E. Golovatch,³⁵ R.W. Gothe,³⁶ K.A. Griffioen,⁴⁴ N. Harrison,³⁸ F. Hauenstein,³² T.B. Hayward,⁴⁴ D. Heddle,^{7,38} K. Hicks,³¹ M. Holtrop,²⁹ Y. Ilieva,³⁶ D.G. Ireland,⁴⁰ E.L. Isupov,³⁵ H.S. Jo,²⁵ S. Johnston,¹ D. Keller,^{43,31} G. Khachatryan,⁴⁵ M. Khachatryan,³² A. Khanal,¹² M. Khandaker,^{30,‡} C.W. Kim,¹⁵ W. Kim,²⁵ F.J. Klein,⁵ V. Kubarovsky,³⁸ S.E. Kuhn,³² L. Lanza,²⁰ M.L. Kabir,²⁸ P. Lenisa,¹⁷ K. Livingston,⁴⁰ I. J. D. MacGregor,⁴⁰ D. Marchand,²² N. Markov,⁸ M. Mayer,³² B. McKinnon,⁴⁰ Z.E. Meziani,³⁷ T. Mineeva,³⁹ M. Mirazita,¹⁸ R.A. Montgomery,⁴⁰ C. Munoz Camacho,²² P. Nadel-Turonski,^{38,5} S. Niccolai,²² A.I. Ostrovidov,¹³ L.L. Pappalardo,¹⁷ R. Paremuzyan,^{29,45} E. Pasyuk,^{38,2} O. Pogorelko,²³ J. Poudel,³² Y. Prok,^{32,43} D. Protopopescu,⁴⁰ M. Ripani,¹⁹ D. Riser,⁸ A. Rizzo,^{20,34} G. Rosner,⁴⁰ P. Rossi,^{38,18} F. Sabatié,⁶ C. Salgado,³⁰ R.A. Schumacher,⁴ Y.G. Sharabian,³⁸ Iu. Skorodumina,^{36,35} D. Sokhan,⁴⁰ O. Soto,³⁹ N. Sparveris,³⁷ S. Strauch,³⁶ M. Taiuti,^{14,§} J.A. Tan,²⁵ N. Tyler,³⁶ M. Ungaro,^{38,8} H. Voskanyan,⁴⁵ R. Wang,²² D.P. Watts,⁴¹ X. Wei,³⁸ L.B. Weinstein,³² M.H. Wood,³ N. Zachariou,⁴¹ J. Zhang,^{43,32} and Z.W. Zhao^{9,36}

(The CLAS Collaboration)

¹Argonne National Laboratory, Argonne, Illinois 60439

²Arizona State University, Tempe, Arizona 85287-1504

³Canisius College, Buffalo, NY

⁴Carnegie Mellon University, Pittsburgh, Pennsylvania 15213

⁵Catholic University of America, Washington, D.C. 20064

⁶IRFU, CEA, Université Paris-Saclay, F-91191 Gif-sur-Yvette, France

⁷Christopher Newport University, Newport News, Virginia 23606

⁸University of Connecticut, Storrs, Connecticut 06269

⁹Duke University, Durham, North Carolina 27708-0305

¹⁰Fairfield University, Fairfield CT 06824

¹¹Università di Ferrara, 44121 Ferrara, Italy

¹²Florida International University, Miami, Florida 33199

¹³Florida State University, Tallahassee, Florida 32306

¹⁴Università di Genova, 16146 Genova, Italy

¹⁵The George Washington University, Washington, DC 20052

¹⁶Idaho State University, Pocatello, Idaho 83209

¹⁷INFN, Sezione di Ferrara, 44100 Ferrara, Italy

¹⁸INFN, Laboratori Nazionali di Frascati, 00044 Frascati, Italy

¹⁹INFN, Sezione di Genova, 16146 Genova, Italy

²⁰INFN, Sezione di Roma Tor Vergata, 00133 Rome, Italy

²¹INFN, Sezione di Torino, 10125 Torino, Italy

²²Institut de Physique Nucléaire, IN2P3-CNRS, Université Paris-Sud, Université Paris-Saclay, F-91406 Orsay, France

²³Institute of Theoretical and Experimental Physics, Moscow, 117259, Russia

²⁴James Madison University, Harrisonburg, Virginia 22807

²⁵Kyungpook National University, Daegu 41566, Republic of Korea

²⁶Lamar University, 4400 MLK Blvd, PO Box 10009, Beaumont, Texas 77710

²⁷LPSC, Université Grenoble-Alpes, CNRS/IN2P3, 38026 Grenoble, France

²⁸Mississippi State University, Mississippi State, MS 39762-5167

²⁹University of New Hampshire, Durham, New Hampshire 03824-3568

³⁰Norfolk State University, Norfolk, Virginia 23504

³¹Ohio University, Athens, Ohio 45701

³²Old Dominion University, Norfolk, Virginia 23529

³³University of Richmond, Richmond, Virginia 23173

³⁴Università di Roma Tor Vergata, 00133 Rome Italy

³⁵Skobeltsyn Institute of Nuclear Physics, Lomonosov Moscow State University, 119234 Moscow, Russia

³⁶University of South Carolina, Columbia, South Carolina 29208

³⁷Temple University, Philadelphia, PA 19122

³⁸Thomas Jefferson National Accelerator Facility, Newport News, Virginia 23606

³⁹Universidad Técnica Federico Santa María, Casilla 110-V Valparaíso, Chile

⁴⁰University of Glasgow, Glasgow G12 8QQ, United Kingdom

⁴¹University of York, York YO10 5DD, United Kingdom

⁴²Virginia Tech, Blacksburg, Virginia 24061-0435

⁴³University of Virginia, Charlottesville, Virginia 22901

⁴⁴College of William and Mary, Williamsburg, Virginia 23187-8795

⁴⁵Yerevan Physics Institute, 375036 Yerevan, Armenia

(Dated: March 2, 2022)

In the past two decades, deeply virtual Compton scattering of electrons has been successfully used to advance our knowledge of the partonic structure of the free proton and investigate correlations between the transverse position and the longitudinal momentum of quarks inside the nucleon. Meanwhile, the structure of bound nucleons in nuclei has been studied in inclusive deep-inelastic lepton scattering experiments off nuclear targets, showing a significant difference in longitudinal momentum distribution of quarks inside the bound nucleon, known as the EMC effect. In this work, we report the first beam spin asymmetry (BSA) measurement of exclusive deeply virtual Compton scattering (DVCS) off a proton bound in ${}^4\text{He}$. The data used here were accumulated using a 6 GeV longitudinally polarized electron beam incident on a pressurized ${}^4\text{He}$ gaseous target placed within the CLAS spectrometer in Hall-B at the Thomas Jefferson National Accelerator Facility. The azimuthal angle (ϕ) dependence of the BSA was studied in a wide range of virtual photon and scattered proton kinematics. The Q^2 , x_B , and t dependencies of the BSA on the bound proton are compared with those on the free proton. In the whole kinematical region of our measurements, the BSA on the bound proton is smaller by 20% to 40%, indicating possible medium modification of its partonic structure.

Electromagnetic probes have played a major role in advancing our knowledge about the structure of the nucleon. While lepton-nucleon elastic scattering measurements have taught us about the spatial charge and magnetization distributions [1, 2], deep-inelastic scattering experiments have uncovered the partonic structure of the nucleon and the longitudinal momentum distributions of the constituent partons, i.e., quarks and gluons [3]. With nuclear targets, deeply inelastic lepton scattering measurements have revealed that the distribution of quarks in a nucleus is not a simple convolution of their distributions within nucleons, an observation known as the ‘‘EMC effect’’ [4] (for reviews on the topic, see [5–8]).

A wealth of information on the structure of hadrons lies in the correlations between the momentum and spatial degrees of freedom of the partons. These correlations can be revealed through deeply virtual Compton scattering (DVCS), i.e., the hard exclusive lepto-production of a real photon, which provides access to a three-dimensional (3-D) imaging of partons within the generalized parton distributions (GPDs) framework [9–13]. The measurement of free proton DVCS has been the focus of a worldwide effort [14–26] involving several accelerator facilities such as Jefferson Lab, DESY and CERN. These measure-

ments now enable the extractions of GPDs and a 3-D tomography of the free proton [27, 28]. New measurements of DVCS from the ${}^4\text{He}$ nucleus are a critical step towards providing a similar 3-D picture of the quark structure of the nucleus [29]. In the nuclear case, however, two channels are available, the coherent channel where the scattering is off the entire nucleus, which is left intact in the final state [30], and the incoherent channel where the DVCS occurs on a nucleon, which is ejected from the nucleus. The latter is the focus of this letter and provides a unique access to the modification of the partonic structure of the bound nucleons [31–33]. The ${}^4\text{He}$ nucleus is an ideal experimental target for this measurement as it is characterized by a strong binding energy, a relatively high nuclear core density, and a large EMC effect [34]. Moreover, it remains simple enough that precise calculation of its structure can be performed, making this nucleus the perfect target for our investigation of the medium modifications of the nucleon’s partonic structure. The previous measurements of DVCS off nuclei, and in particular off ${}^4\text{He}$, performed at HERMES [35] yielded results with both ‘‘coherent enriched’’ and ‘‘incoherent enriched’’ event samples, hence not fully exclusive, but significant enough to be compared with our results below.

In this Letter, we present the first exclusive measurement of the beam-spin asymmetry (BSA) in deeply virtual electroproduction of a real photon off a bound proton in ${}^4\text{He}$. Fig. 1 illustrates the leading-twist handbag diagram for the DVCS process. In the Bjorken regime, i.e. large virtual photon four-momentum squared ($Q^2 = -q^2 = -(k - k')^2$), and at small invariant mo-

*Current address: The George Washington University, Washington, DC 20052

†Current address: Imam Abdulrahman Bin Faisal University, Industrial Jubail 31961, Saudi Arabia

‡Current address: Idaho State University, Pocatello, Idaho 83209

§Current address: INFN, Sezione di Genova, 16146 Genova, Italy

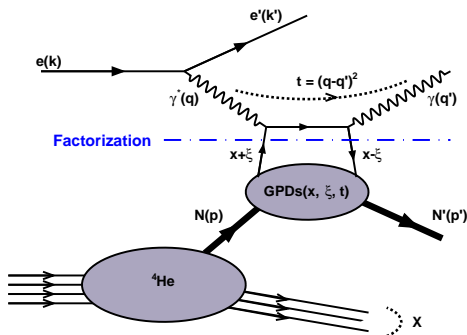


FIG. 1: Representation of the leading-order, twist-2, hand-bag diagram of the incoherent DVCS process off ${}^4\text{He}$, where the four-vectors of the electrons, photons, and protons are denoted by k/k' , q/q' , and p/p' , respectively. $x+\xi$ is the nucleon longitudinal momentum fraction carried by the struck quark, -2ξ is the longitudinal momentum fraction of the momentum transfer Δ ($= q - q'$), and t ($= \Delta^2$) is the squared momentum transfer between the initial and the final state nucleon.

mentum transfer ($t = (q - q')^2$), the DVCS scattering process can be factorized, leaving the non-perturbative structure of the nucleon to be parameterized in terms of four chirally even GPDs: H , E , \tilde{H} , and \tilde{E} , representing the four helicity-spin combinations of the quark-nucleon states [36, 37]. Experimentally, we measure the squared sum of the Bethe-Heitler (BH) and the DVCS amplitudes. The BH process, where the real photon is emitted by the incident or the scattered electron rather than the nucleon, dominates the cross section at our kinematics. The BSA arises from the interference of these two terms and is directly sensitive to the DVCS amplitude that contains the information on the GPDs. Using a longitudinally polarized electron beam (L) and an unpolarized target (U), the BSA is defined as:

$$A_{LU} = \frac{d^5\sigma^+ - d^5\sigma^-}{d^5\sigma^+ + d^5\sigma^-}, \quad (1)$$

where $d^5\sigma^+$ ($d^5\sigma^-$) is the virtual photoproduction differential cross section for a positive (negative) beam helicity.

Following the cross section decomposition provided in [38], the different components can be expressed in terms of Fourier coefficients associated with ϕ -harmonics, where ϕ is the angle between the leptonic and the hadronic planes of the reaction. At leading-twist, the BSA can be parameterized as:

$$A_{LU}(\phi) = \frac{a_0 \sin(\phi)}{1 + a_1 \cos(\phi) + a_2 \cos(2\phi)}, \quad (2)$$

where the parameters $a_{0,1,2}$ are combinations of the aforementioned Fourier coefficients. The $\sin(\phi)$ harmonic is dominant in A_{LU} and is proportional to the following combination of Compton form factors (CFF) \mathcal{H} , \mathcal{E} , and

$\tilde{\mathcal{H}}$ as [27]

$$a_0 \propto \text{Im}(F_1 \mathcal{H} - \frac{t}{4M^2} F_2 \mathcal{E} + \frac{x_B}{2} (F_1 + F_2) \tilde{\mathcal{H}}), \quad (3)$$

where F_1 and F_2 are the Dirac and Pauli form factors, respectively, and x_B the Bjorken scaling variable. The real and the imaginary parts of the CFF \mathcal{H} relate to the GPD H as

$$\Re(\mathcal{H}) = \mathcal{P} \int_0^1 dx [H(x, \xi, t) - H(-x, \xi, t)] C^+(x, \xi), \quad (4)$$

$$\Im(\mathcal{H}) = -\pi [H(\xi, \xi, t) - H(-\xi, \xi, t)], \quad (5)$$

with \mathcal{P} the Cauchy principal value integral and C^+ a coefficient function defined as $(1/(x - \xi) + 1/(x + \xi))$, where ξ is the skewing factor and can be related to x_B by $\xi \approx \frac{x_B}{2 - x_B}$. Similar expressions apply for the GPDs E , \tilde{H} , and \tilde{E} [27]. At the forward limit, $\xi \rightarrow 0$ and $t \rightarrow 0$, the GPD H reduces to quark, anti-quark PDFs, and its zeroth moment in x represents the elastic Dirac form-factor F_1 .

The experiment (E08-024 [39]) took place in Hall-B of Jefferson Lab using the nearly 100% duty factor, longitudinally polarized electron beam (83% polarization) from the Continuous Electron Beam Accelerator Facility (CEBAF) at an energy of 6.064 GeV. The data were accumulated over 40 days using a 6-atm-pressure, 292-mm-long, and 6-mm-diameter gaseous ${}^4\text{He}$ target centered 64 cm upstream of the CEBAF Large Acceptance Spectrometer (CLAS) coordinate center. For DVCS experiments, the CLAS baseline design [40] was supplemented with an inner calorimeter (IC) and a solenoid magnet. The IC extended the photon detection acceptance of CLAS down to a polar angle of 4° . The 5-Tesla solenoid magnet in the center of which the target was located prevented the high-rate low-energy Møller electrons from reaching the CLAS drift chambers by guiding these electrons inside a tungsten shield placed around the beamline.

Incoherent DVCS events were selected by requiring an electron, a proton, and at least one photon in the final state using the standard particle identification framework of the CLAS event reconstruction (see [41] for additional details on the particle identification). Note that even though the DVCS reaction has only one real photon in the final state, events with more than one photon were not discarded at this stage. These extra photons were mostly soft photons from accidental coincidence which, as will be discussed below, the DVCS exclusivity cuts easily eliminated. In the following stage, the most energetic photon was considered as the DVCS photon candidate.

Further requirements were applied to clean the identified initial set of incoherent DVCS events from accidental and physics background events. First, events were selected with Q^2 greater than 1 GeV^2 and the γ^*p invariant mass ($W = \sqrt{(q + p)^2}$, assuming that the initial

nucleon is at rest) greater than 2 GeV. This is a commonly accepted region of kinematics used by the previous DVCS experiments and avoids the nucleon resonance region. The squared transferred momentum to the recoil proton t , calculated from the four-momentum vectors of the incoming and outgoing photons, was required to be greater than a minimum kinematically allowed value (t_{min}) at given Q^2 and W defined as:

$$t_{min} = -Q^2 \frac{2(1 - x_B)(1 - \sqrt{1 + \epsilon^2}) + \epsilon^2}{4x_B(1 - x_B) + \epsilon^2}, \quad (6)$$

where $\epsilon^2 = \frac{4M_p^2 x_B^2}{Q^2}$ and M_p is the proton mass. This cut was applied to avoid accepting events that appear in unphysical regions of kinematics due to detector resolution and radiative effects. We specifically use the kinematics of the photons to determine t because the initial proton kinematics is unknown due to Fermi motion.

In the final sample, the exclusivity of the incoherent DVCS events was ensured by imposing a series of constraints based on the four-momentum conservation in the reaction $ep \rightarrow e'p'\gamma$. These kinematical variables are: the coplanarity angle $\Delta\phi$ between the (γ, γ^*) and (γ^*, p') planes, the missing energy, mass, and transverse momentum of the $e'\gamma$ and $e'p'\gamma$ systems, the missing mass squared of the $e'p'$ system, and the angle θ between the measured photon and the missing momentum of the $e'p'$ system. The experimental distributions for the most relevant exclusivity variables are shown in Fig. 2. Because of the Fermi motion of the nucleons in the helium nucleus, the cuts indicated by the dashed lines are slightly wider than those previously used for free proton experiments [21]. After the corrections discussed below, the asymmetries appear to be stable as a function of cut width and we saw no sizable effect that could be related to the initial momentum of the nucleons. We also rejected events where a π^0 was identified by the invariant mass of two photons. At the end of this selection process, about 30k events passed all the requirements.

The two main backgrounds that contributed to the event sample after the exclusivity cuts are due to accidental coincidences and exclusive π^0 production where one of the photons from the π^0 decay escapes detection. The contribution from accidental events, i.e., $e'p'\gamma$ collections with particles originating from different electron scatterings, was evaluated to be 6.5% by selecting events passing all our selection cuts but originating from different vertices. The π^0 contamination was estimated and subtracted using detector simulation and experimental data. From simulation, we calculated the ratio ($R = N_{sim}^{1\gamma}/N_{sim}^{2\gamma}$) of the number of π^0 events that were wrongly identified as exclusive $ep \rightarrow e'p'\gamma$ events ($N_{sim}^{1\gamma}$) to the number of events correctly identified as exclusive $ep \rightarrow e'p'\pi^0$ ($N_{sim}^{2\gamma}$). Then in each kinematical bin and for each beam-helicity state, the π^0 -subtracted experimental DVCS events were calculated

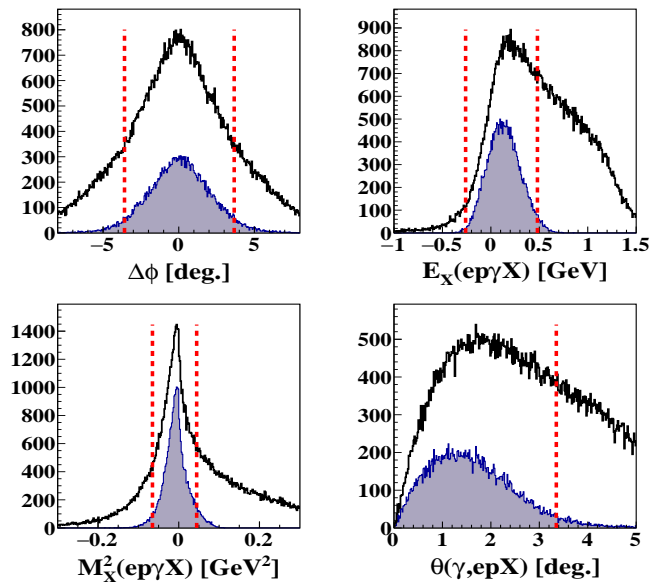


FIG. 2: The distributions from left to right and from top to bottom are: $\Delta\phi$, missing energy, missing mass squared and the cone angle (θ) between the measured and the calculated photons in the $e'p'$ final-state system. The incoherent DVCS exclusivity cuts are represented by the vertical red-dashed lines. The black distributions represent the incoherent DVCS event candidates before the exclusivity cuts. The shaded distributions represent the incoherent DVCS events that passed all of these cuts except the quantity plotted.

as $N = N_{exp}^{ep \rightarrow e'p'\gamma} - R N_{exp}^{ep \rightarrow e'p'\pi^0}$, where $N_{exp}^{ep \rightarrow e'p'\gamma}$ ($N_{exp}^{ep \rightarrow e'p'\pi^0}$) is the number of the experimentally identified $ep \rightarrow e'p'\gamma$ ($ep \rightarrow e'p'\pi^0$) events. Depending on the kinematics, we subtracted between 8 and 10% of the data due to the π^0 contamination.

Experimentally, A_{LU} is defined as

$$A_{LU} = \frac{1}{P_B(1 - C)} \frac{N^+ - N^-}{N^+ + N^-}, \quad (7)$$

where N^+ and N^- are the number of DVCS events for the positive and negative beam-helicity states, P_B is the longitudinal beam polarization, and C stands for the contamination percentage of the accidental coincidences.

In the kinematical phase-space of our experiment, the ϕ dependence of A_{LU} is most sensitive to the imaginary part of the CFFs through the a_0 term of Eq. 2, as confirmed by high statistics measurements on the free proton [21, 26]. In the determination of a_0 in Eq. 3, the CFF \mathcal{E} and \mathcal{H} are suppressed due to form-factors and the smallness of the coefficients. Therefore, the dominant contribution to the BSA comes from the CFF \mathcal{H} and hence the GPD H .

Due to limited statistics, the data were binned two-dimensionally into 36 bins. That is, four bins in one of the kinematical variable of interest (Q^2 , x_B , or t) and then nine bins in the azimuthal angle (ϕ). Fig. 3 presents

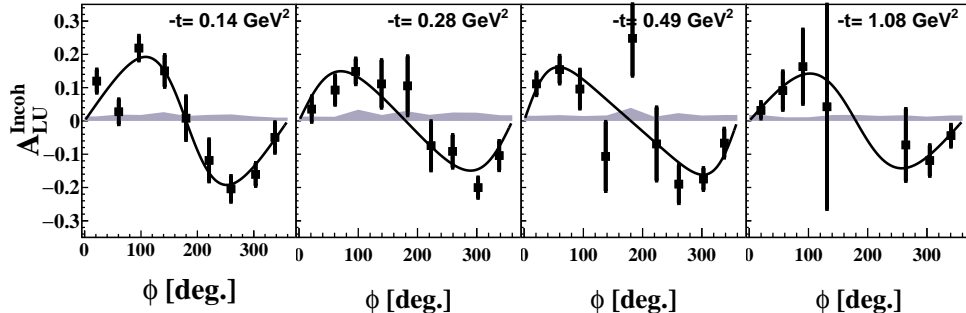


FIG. 3: The incoherent A_{LU} as a function of ϕ for different t bins. The error bars represent the statistical uncertainties. The gray bands represent the systematic uncertainties, including the normalization uncertainties. The black curves are the results of our fits with the form $\frac{a_0 \sin(\phi)}{1+a_1 \cos(\phi)}$.

the measured incoherent A_{LU} as a function of ϕ in bins of t (integrated over the full Q^2 and x_B ranges). The curves on the plots are fits of the form $\frac{a_0 \sin(\phi)}{1+a_1 \cos(\phi)}$. The main contributions to systematic uncertainties on these fits are from the choice of the DVCS exclusivity cuts (6%) and the large bin size (7%). The systematic uncertainties sum up to less than 10% for all data points and thus always remain significantly smaller than the statistical uncertainties.

Fig. 4 presents the dependence of the fitted A_{LU} values at $\phi = 90^\circ$ (a_0 parameter from the individual fits in Fig. 3) on the kinematical variables Q^2 , x_B , and t . Within the given uncertainties, A_{LU} does not show a strong dependence on Q^2 . The x_B and t dependencies are compared to the theoretical calculations performed by S. Liuti and K. Taneja [31]. Their model uses a nuclear spectral function and considers mainly the effect of the nucleon off-shellness. The calculations are carried out at slightly different kinematics than our data but still provide important guidance. The experimental results appear to have smaller asymmetries especially at small x_B than the calculations. These differences may arise from nuclear effects that are not taken into account in the model, such as long-range interactions and final state interactions of the knocked-out proton. On the graph for the $-t$ dependence, we show previous measurements by HERMES collaboration [35], in which only electrons and photons were measured. Due to the large experimental uncertainties of the HERMES points, the two measurements are completely compatible.

One can use the nuclear DVCS to measure a “generalized” EMC effect in order to see if significant nuclear effects are also visible within the GPD framework. To explore this idea, we constructed the ratio of A_{LU} for bound protons to that on a free proton target. Fig. 5 presents the BSA ratio based on interpolation of the free proton asymmetries from CLAS [21] as a function of the kinematical variable t . The A_{LU} ratios show 25%-40% lower asymmetries that are independent of t for a bound

proton compared to the free proton. The measurements disagree with the off-shell [31] and the on-shell calculations that use the medium-modified GPDs as calculated from the quark-meson coupling model [33]. Our results show that an important nuclear effect is missing from the existing models in order to explain this strong quenching of the BSA. More theoretical developments will be needed to identify the origin of this quenching, in particular it will be important to differentiate initial from final state effects and how they affect the DVCS asymmetries.

In summary, we have presented the first BSA measurement associated with bound proton DVCS off ^4He using an upgraded setup of the CLAS spectrometer at Jefferson Lab. Our results are compared to model calculations based on different assumptions of the nuclear medium effects at the partonic level. The bound-proton BSA is largely suppressed compared to the free proton BSA. This result is a first step in using a novel experimental method of understanding the properties of bound nucleons directly from the basic degrees of freedom of QCD, quarks and gluons. Planned experiments at Jefferson Lab will continue and extend these studies of the bound nucleon structure using DVCS. We have an experimental program called ALERT using the CLAS12 detector in the Hall-B of Jefferson Lab. These experiments will improve the DVCS measurements with the detection of nuclear fragments to better control the final state interactions and the initial state kinematics of the bound nucleon.

The authors acknowledge the staff of the Accelerator and Physics Divisions at the Thomas Jefferson National Accelerator Facility who made this experiment possible. This work was supported in part by the Chilean Comisión Nacional de Investigación Científica y Tecnológica (CONICYT), by CONICYT PIA grant ACT1413, the Italian Istituto Nazionale di Fisica Nucleare, the French Centre National de la Recherche Scientifique, the French Commissariat à l’Energie Atomique, the U.S. Department of Energy under Contract No. DE-AC02-06CH11357, the

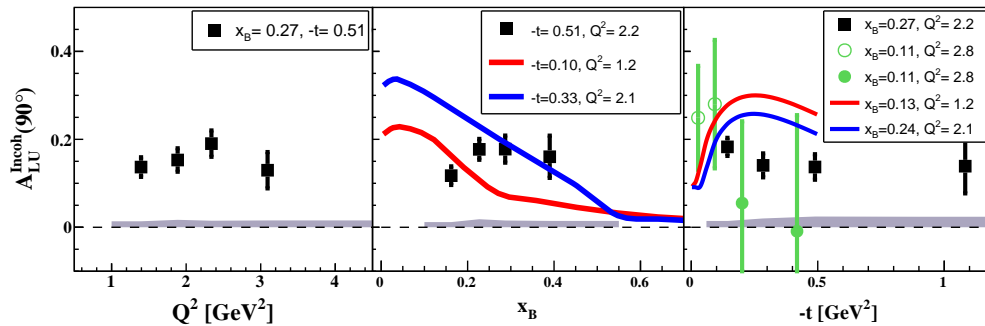


FIG. 4: The Q^2 (left), x_B (middle), and t dependencies (right) of the fitted A_{LU} at $\phi = 90^\circ$ (black squares). The error bars represent the statistical uncertainties, while the gray bands represent the systematic uncertainties. On the middle plot the curves are theoretical calculations from [31]. On the right plot the solid (empty) green circles are the HERMES $-A_{LU}$ (a positron beam was used) inclusive measurements for the incoherent (coherent) enriched region [35]; the curves represent theoretical calculations from [31].

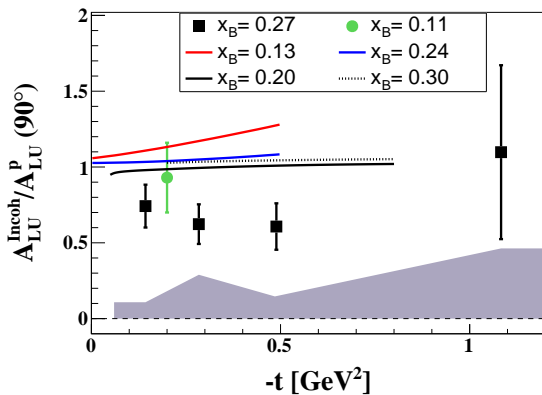


FIG. 5: The A_{LU} ratio of the bound to the free proton at $\phi = 90^\circ$ as a function of t . The black squares are from this work, the green circle is the HERMES measurement [35]. The error bars represent the statistical uncertainties, while the gray band represents the systematic uncertainties. The blue and red curves are results of off-shell calculations [31]. The solid and dashed black curves are from on-shell calculations [33].

United Kingdom Science and Technology Facilities Council (STFC), the Scottish Universities Physics Alliance (SUPA), the National Research Foundation of Korea, and the Office of Research and Economic Development at Mississippi State University. M. Hattawy also acknowledges the support of the Consulat Général de France à Jérusalem. The Southeastern Universities Research Association operates the Thomas Jefferson National Accelerator Facility for the United States Department of Energy under Contract No. DE-AC05-06OR23177.

- [1] R. Hofstadter and R. W. McAllister, Phys. Rev. **98**, 217 (1955).
- [2] C. F. Perdrisat, V. Punjabi and M. Vanderhaeghen, Prog. Part. Nucl. Phys. **59**, 694 (2007).
- [3] M. Tanabashi *et al.* (Particle Data Group), Phys. Rev. D **98**, 030001 (2018).
- [4] J. J. Aubert *et al.*, Phys. Lett. vol. B **123**, pp. 275278 (1983).
- [5] M. Arneodo, Phys. Rept. **240**, 301 (1994).
- [6] D. F. Geesaman, K. Saito and A. W. Thomas, Ann. Rev. Nucl. Part. Sci. **45**, 337 (1995).
- [7] P. R. Norton, Rept. Prog. Phys. **66**, 1253 (2003).
- [8] O. Hen *et al.*, Rev. Mod. Phys. **89**, no. 4, 045002 (2017).
- [9] D. Mueller, D. Robaschik, B. Geyer, F.M. Dittes, and J. Horejsi, Fortsch. Phys. **42**, 101 (1994).
- [10] X.D. Ji, Phys. Rev. Lett. **78**, 610 (1997).
- [11] X.D. Ji, Phys. Rev. D **55**, 7114 (1997).
- [12] A.V. Radyushkin, Phys. Lett. B **380**, 417 (1996).
- [13] A.V. Radyushkin, Phys. Rev. D **56**, 5524 (1997).
- [14] S. Stepanyan *et al.* [CLAS Collaboration], Phys. Rev. Lett. **87**, 182002 (2001).
- [15] A. Airapetian *et al.* [HERMES Collaboration], Phys. Rev. Lett. **87**, 182001 (2001).
- [16] A. Airapetian *et al.* [HERMES Collaboration], Phys. Rev. D **75**, 011103 (2007).
- [17] S. Chekanov *et al.* [ZEUS Collaboration], Phys. Lett. B **573**, 46 (2003).
- [18] A. Aktas *et al.* [H1 Collaboration], Eur. Phys. J. C **44**, 1 (2005).
- [19] S. Chen *et al.* [CLAS Collaboration], Phys. Rev. Lett. **97**, 072002 (2006).
- [20] M. Defurne *et al.* [Jefferson Lab Hall A Collaboration], Phys. Rev. C **92**, no. 5, 055202 (2015).
- [21] F.X. Girod *et al.* [CLAS Collaboration], Phys. Rev. Lett. **100**, 162002 (2008).
- [22] M. Mazouz *et al.* [Jefferson Lab Hall A Collaboration], Phys. Rev. Lett. **99**, 242501 (2007).
- [23] G. Gavalian *et al.* [CLAS Collaboration], Phys. Rev. C

- 80**, 035206 (2009).
- [24] E. Seder *et al.* [CLAS Collaboration], Phys. Rev. Lett. **114**, 032001 (2015).
- [25] S. Pisano *et al.* [CLAS Collaboration], Phys. Rev. D **91**, 052014 (2015).
- [26] H. S. Jo *et al.* [CLAS Collaboration], Phys. Rev. Lett. **115**, no. 21, 212003 (2015).
- [27] M. Guidal, H. Moutarde, and M. Vanderhaeghen, Rep. Prog. Phys. **76**, 066202 (2013).
- [28] R. Dupré, M. Guidal and M. Vanderhaeghen, Phys. Rev. D **95**, no. 1, 011501 (2017).
- [29] R. Dupré and S. Scopetta, Eur. Phys. J. A **52**, no. 6, 159 (2016).
- [30] M. Hattawy *et al.* [CLAS Collaboration], Phys. Rev. Lett. **119**, no. 20, 202004 (2017).
- [31] S. Liuti and K. Taneja, Phys. Rev. C **72**, 032201 (2005).
- [32] V. Guzey and T. Teckentrup, Phys. Rev. D **74**, 054027 (2006)
- [33] V. Guzey, A. W. Thomas and K. Tsushima, Phys. Lett. B **673**, 9 (2009).
- [34] J. Seely *et al.*, Phys. Rev. Lett. **103**, 202301 (2009).
- [35] A. Airapetian *et al.* [HERMES Collaboration], Phys. Rev. C **81**, 035202 (2010).
- [36] J.C. Collins and A. Freund, Phys. Rev. D **59**, 074009 (1999).
- [37] X.-D. Ji and J. Osborne, Phys. Rev. D **58**, 094018 (1998).
- [38] A. V. Belitsky, D. Mueller and A. Kirchner, Nucl. Phys. B **629**, 323 (2002). Updated in: A. V. Belitsky and D. Mueller, Phys. Rev. D **82**, 074010 (2010).
- [39] K. Hafidi *et al.*, proposal PR-08-024 to JLab PAC33 (https://www.jlab.org/exp_prog/proposals/08/PR-08-024.pdf).
- [40] B. A. Mecking *et al.*, Nucl. Instrum. Meth. A **503**, 513 (2003).
- [41] M. Hattawy, Ph.D. thesis, Université Paris Sud - Paris XI, France, 2015 [Institution Report No. 2015PA112161].